LAMINAR HEAT TRANSFER CHARACTERISTICS OF A PLATE-LOUVER FIN SURFACE OBTAINED BY THE DIFFERENTIAL FLUID ENTHALPY METHOD

by

Branislav BAČLIĆ, Dušan GVOZDENAC and Dušan SEKULIĆ

Original scientific paper
UDC: 536.24:66.045.1=20
BIBLID: 0354–9836, *1* (1997), 1, 93–108

In order to establish the Colburn factor vs Reynolds number correlation from single blow experimental data of a particular plate-fin surface, the Differential Fluid Enthalpy Method (DFEM) has been applied. This method overcomes the deficiencies of previously known methods and simply deals with the realistic exponential inlet temperature signal. In this paper the method is modified to enable simultaneous determination of the test matrix specific heat as well. The correlation obtained is based on one hundred experimental runs covering the range 385 < Re < 1930. The compact surface sample has been cut out by electro-erosion from a completely manufactured (brased aluminum) crossflow heat exchanger core. For completeness, the corresponding Fanning factor results are included in the paper.

Introduction

This paper presents a continuation of presenting our experience in developing a new experimental facility for testing compact heat exchanger surfaces at the University of Novi Sad. The description of the apparatus and its performance identification method are given in Bačlić *et al.*, [1]. The present paper serves two main purposes: (1) to determine the laminar heat transfer and flow friction characteristics of a particular plate-louver fin surface, and (2) to describe the data reduction procedure that enables the simultaneous determination of the fluid-to-surface number of heat transfer units and the test matrix specific heat.

In has been discussed in [1] that the design of the apparatus, the operating conditions and the test matrix sampling method were selected to satisfy some specific requirements and the reader should refer to the introductory remarks given there. The theory presented here is discussed relative to its application to the test facility, to the test core sample and to the data reduction procedure. The method used to reduce the data, the *D*ifferential *F*luid *E*nthalpy *M*ethod (DFEM) [2], is modified to enable the determination of the test core specific heat.

First the test core description is given and then the DFEM is discussed. This is followed by the explanation of the data reduction procedure and finally the test surface characteristics are presented as obtained from one hundred experimental runs.

The test core

The compact surface sample has been cut by electroerosion from a completely manufactured (brazed aluminum) crossflow heat exchanger core as presented in Fig. 1. This particular heat exchanger is used in a standard aircraft cabin pressurizing and air conditioning system. The cylindrical core sample is 105 mm in diameter having a length of L = 93.5 mm which is the actual core length in the air flow direction on the side being tested. The matrix has been cut to fit the inside diameter of the apparatus test section and is to be inserted there at the location indicated in Fig. 2 of [1].

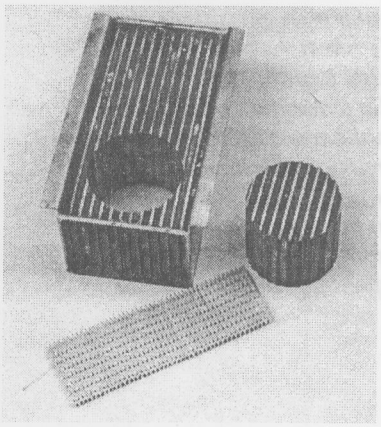

Figure 1. A view of the test sample being cut out of the heat exchanger core and the fin surface sample

The core side tested is a plate-step louver fin surface with the following geometrical parameters: fin pitch = 578.4 per m, plate spacing = 7.2 mm, louver spacing = 9.5 mm, louver gap = 1.2 mm, flow passage hydraulic diameter diameter = 2.563 mm, fin metal thickness = 0.15 mm, total heat transfer area/volume between plates = 1421 m^{-1}, fin area/total area = 0.8141, free flow area/frontal area = 0.5916. Prior to the cutting, the core was inspected for manufacturing malformations. The visual inspection of the completely manufactured core indicated the existence of nonuniform passages originating from several reasons like distortions of various types and fin-spacing type nonuniformities. Somewhat shorter fin specings, due to squeezing the fin surface in serial assembling procedure, have been noticed edgewise the frontal area. However, the individual passage areas on the average do not deviate significantly from the nominal passage area. The surface geometrical characteristics of the side being tested, as given above, have been obtained as average quantities for a particular core selected randomly from the production line. When compared with idealized geometrical characteristics, that have been intended by the tool and die design, some deviations were obvious. For example, a well shaped design is intended to provide a louver gap of 0.9 mm and a fin pitch of 571.4 per m. Theway of test core sampling as described is believed to eliminate any major influence that manufacturing tolerances could have in positioning the j-Re characteristics.

The usage of such a test core sample as a thermal energy storage matrix raised some additional problems. Namely, the other (no flow) side of the core, consisting of rectangular plan fin-plate surface, when mounted in the apparatus test section, has

trapped a certain amount of ambient air among the straight continuous fins. The matrix was surrounded by sealing tape to prevent transverse conduction to the test section wall as to prevent the by-pass leakage. The spealing tape was acting also as a protector of the soft, easily eformable, thin fin surfaces (left after electro-erosion cutting) during the handling and insertion of the test core into the apparatus test section. Transient heating of the test matrix, which is thus, a kind of a corrugated sandwich structure with cellular layers filled by air, produces complicated interactions. High thermal conductivity of aluminum tends to create a uniform solid temperature distribution so that the air being trapped is quickly exposed to the onset of free convection in the cells. A lumped thermal capacity of such a test matrix can not be reliably predicted so it is left to be determined from the same experimental data utilized for the determination of the basic heat transfer characteristics. Thisfact makes the present data reduction procedure quite novel.

A need for experimental determination of the test matrix *effective* specific heat can be also supported by the conclusions that have been derived in the solid density determination. The solid density $\rho_B = 2447$ kg/m^3 obtained from the core mass $m_B = 0.4134$ kg and the core solid material volume (measured on the Archimedes' principle as the weight of the water displaced by the test sample) indicates that the presence of the brazing material has a significant influence in lowering the value of the basic core material (99.5% Al) density. Significant influence can thus be expected on the value of the specific heat. Just to note that the same measurements showed that the test sample porosity (including voids on both sides) can be estimated as 0.7914. The mass of air being trapped in the matrix cells on the no-flow side is negligible, but its specific heat being higher than that of aluminum will contribute to the effective test matrix thermal capacity. Therefore, to avoid a speculative prediction of the test matrix effective specific heat, that has to be based on the study of aluminum-brazing material-cells interactions, an experimental identification of such a "property" was realized.

The trial reproductibility runs were conducted both with large intervals between individual runs and by repeating runs one immediately following the other. What appeared was an additional consequence of air being present in the matrix cells. Namely, it affected the fulfillment of the matrix initial temperature condition, and this has proved to have the most influence on the c_s values obtained from the data reduction procedure. At the same time there was no *significant influence on the NTU values* obtained in different runs using the same flow rate. This proved that the effective specific heat of the test core should be regarded as a process parameter rather than a material property, and that its simultaneous determination with the heat transfer characteristics should be regarded as *an elimination procedure* of an unsusceptible to reliable prediction parameter.

Differential fluid enthalpy method

DFEM is a new variant of the single-blow (steady flow is established before the change in temperature-time trace not just of the exit fluid from the test core, but of the inlet fluid as well. Previous experimentalistis often connected the thermopiles located upstream of the electric heather and downstream from the test matrix to provide a reading

of temperature difference across the test section. However, none of them came to the simple idea to the result obtained by the fluid capacity rate in order to obtain the differential fluid enthalpy change up to a particular instant. Such an experimentally measured quantity can be easily related to the parameters of the model to provide means for basic heat transfer characteristics determination over the *entire range of the number of heat transfer units* and for *arbitrary inlet fluid temperature variations.*

Consider the dimensionless fluid temperature versus dimensionless time graphs presented in Fig. 2. Steady fluid temperature T_{min} upstream of the heater corresponds to zero dimensionless temperature ($\theta = 0$), while zero dimensionless time ($\eta = 0$) corresponds to the zero matrix local time ($\tau_M = 0$). Let x be the spatial coordinate measured along the matrix in the flow direction so that $0 \le \xi = x/L \le 1$ is its dimensionless range corresponding to the matrix inlet and outlet. Then $\theta(0, \eta)$ and $\theta(1, \eta)$ in Fig. 2 are dimensionless fluid temperature histories at the matrix inlet and outlet, respectively.

In Fig. 2(a) the vertical distance between two curves is the temporal (at any particular instant η^*) difference between the inlet and outlet fluid temperatures. This difference can be measured directly in any experiment and the area between the curves up to any particular point in time can be evaluated as the integral being shown pictorially in Fig. 2(d). This integral is the total dimensionless fluid enthalpy change between the test core inlet and outlet up to any particular instant η^*. Similarly, the total dimensionless fluid enthalpy change in the apparatus test section upstream of the matrix is the are a presented in Fig. 2(b). The area that is shown in Fig. 2(c) is the fraction of the total fluid enthalpy change that has not been absorbed by the test matrix.

The simple idea of the DFEM is that these integrals are to be evaluated from the experimental data and then related to the parameters involved in the mathematical representation of the model describing the transient heating of the test matrix. This can be done in principle for any mathematical model consistent with the underlying basic assumptions.

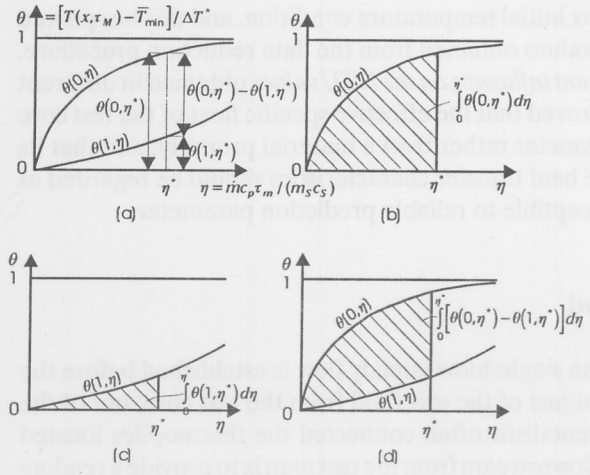

Figure 2. Differential fluid enthalpy representation

The most frequently used mathematical model of transient heat transfer between a fluid flowing through a test core is the, now classical, Anzelius-Schumann model:

$$C_m^* \frac{\partial \theta}{\partial \eta} + \frac{\partial \theta}{\partial \xi} + NTU(\theta - \theta_S) = 0 \tag{1}$$

$$C_m^* \frac{\partial \theta}{\partial \eta} + \frac{\partial \theta}{\partial \xi} + \frac{\partial \theta_S}{\partial \eta} = 0 \tag{2}$$

with both fluid and solid matrix temperatures initially uniform:

$$\theta(\xi,0) = \theta_S(\xi,0) = 0 \tag{3}$$

Contrary to the idealized step change in the inlet fluid temperature, one should modify the model by considering a realistic exponential inlet fluid temperature change:

$$\theta(0,\eta) = 1 - e^{-\frac{\eta}{\eta_0}} \tag{4}$$

It has been shown by Bačlić *et al.* [2] that the integral presented in Fig. 2(d) is related to the parameters involved in the mathematical representation, Eqs. (1) to (4), as:

$$\frac{1}{\eta^*}\int_0^{\eta^*}[\theta(0,\eta) - \theta(1,\eta)]d\eta + \frac{\eta_0}{\eta^*}[\theta(0,\eta^*) - \theta(1,\eta^*)] = 1 - \frac{V_2(NTU, \eta^* NTU)}{\eta^* NTU} \tag{5}$$

for $\eta^* \geq C_m^* \to 0$. The resident fluid to solid matrix thermal capacity $C_m^* = (m_f c_p)/(m_S c_S)$ ratio can be usually neglected due to the fact that the air mass occupying the flow passage volume of the matrix is very small. (In the present experiments: $C_m^* = 0.0014$). Explicit relation for V_2 function appearing in Eq. (5) is given in the Appendix in terms of modified Bessel functions. The right hand side of Eq. (5) is functionally identical to the expression defining the single pass crossflow (both fluids unmixed) heat exchanger effectiveness in terms of the overall number of heat transfer units and capacity rate ratio as given in Bačlić and Heggs [3] by equation (68) or any of the equations (74) through (80), or Eq. (82), or Eq. (83). The numerical values of the RHS of the above equation (5) are tabulated in Table 2 of Bačlić and Heggs [3] for $NTU \leq 10$ and $\eta^* \leq 1$.

In a previous paper Bačlić *et al.*, [2] a recommendation for choosing $\eta^* = 1$ has been given for the data reduction procedure, together with the corresponding chart relating the differential fluid enthalpy change to the number of heat transfer units in the range $10^{-2} \leq NTU \leq 10^3$ which covers more than all practical values. The choice of $\eta^* = 1$ not only simplifies the data reduction procedure, but physically corresponds to the time at which the thermal capacitance of the mass of gas that has entered the test

section is equal to the heat capacitance of the solid matrix. However, in principle there are no restrictions on choosing arbitrary $\eta^* > 1$ value for the data reduction procedure. As presented by Bačlić *et al.* (1986b). DFEM was intended just for experimental determination of *NTU*. In the next section a data reduction procedure that utilizes two distinct η^* values for the evaluation of the experimental values of both *NTU* and c_B is described.

Here it should be emphasized that, when applied to the inlet temperature signal, Eq. (4), (see also Fig. 2(b)), the same principle of the DFEM yields.

$$\frac{1}{\eta^*}\int_0^{\eta^*}\theta(0,h)d\eta+\frac{\eta_0}{\eta^*}\theta(0,\eta^*)=1 \tag{6}$$

This time invariant relation was a key result in the apparatus test section parameters identification (refer to Eq. (16) in [1].

Now subtract Eq. (5) from the Eq. (6) to obtain:

$$\frac{1}{\eta^*}\int_0^{\eta^*}\theta(1,\eta)d\eta+\frac{\eta_0}{\eta^*}\theta(1,\eta^*)=\frac{V_2(NTU,\eta^*NTU)}{\eta^*NTU} \tag{7}$$

which is a DFEM result for the outlet temperature signal. Note that since the common divider η^* drops out from this equation, the leading term becomes the area presented in Fig. 2(c). This result means that the data reduction producer can be based just on the fluid temperature difference measured across the whole test section (*without* measuring the fluid temperature history at the matrix entrance), if and only if the apparatus performatrix entrance), if and only if the apparatus performance can be reliably predicted. This becomes more obvious if one rewrites Eq. (7) in the dimensional form:

$$\frac{\dot{m}c_p}{m_S c_S \Delta T^*}\left\{\int_0^{\tau_m^*}[(L,\tau_m)-\overline{T}_{\min}]d\tau_m+\tau_0[T(L,\tau_m^*)-\overline{T}_{\min}]\right\}=$$

$$=V_2\left(NTU,\frac{\dot{m}c_p\tau_m^*}{m_S c_S}NTU\right)/NTU \tag{8}$$

Suppose that an experimentalist wishes to determine *NTU* from this equation. In essence he must evaluate its complete LHS on the basis of measurements $(T,\overline{T}_{\min},L,\tau_m,\dot{m},m_S)$ and predictions $(c_p,c_S,\tau_0,\Delta T^*)$. The temporal fluid temperature difference appearing in Eq. (8) is measured continuously after the heater has been turned on. The integral in Eq. (8) can be obtained by numerical integration using, say, the trapesoidal rule for equally spaced time intervals. The other term on the LHS of Eq. (8) is obtainable by multiplying the temperature difference at τ_0' by the value of τ_0. However, the time constant τ_0 of the inlet temperature signal is dependent upon the flow

rate, the heat capacity of the heater and other apparatus test section peculiarities. It is thus a performance characteristic of the apparatus and should be known over the flow rate range of interest. The flow rate through the test section is measured and the fluid properties areevaluated on-line, so that the apparatus Reynolds number is known. Having a $\tau_0 - \mathrm{Re}_a$ relation as it was established in [1], one can predict reliably τ_0 without measuring the inlet fluid temperature variation. Similar situation is with the normalizing temperature difference ΔT^* of the test core hat transfer model, which is *not* the maximum temperature difference $\Delta T_{\max}$ of the experiment. Namely, due to the finite fluid-to-wall heat transfer, among these two quantities the following relation holds:

$$\Delta T^* = \Delta T_{\max} \mathrm{e}^{-\frac{NTU_a L_{m1}}{L_2}} \tag{9}$$

since $\Delta T_{\max}$ generated at the heater location is attenuated as shown in [1]. Both NTU_a and $\Delta T_{\max}$ can be reliably predicted for any particular Re_a value if the apparatus performance characteristics are established prior to the core testing as described in [1]. Thus, in addition to the fluid temperature-time trace measurements at the test core exit, the mass flow rate ($\dot{m}$) measurements and the fluid properties evaluation play a major role in the application of the DFEM.

Next section describes the utilization of the Eq. (8) for data reduction procedure when both NTU and c_S are unknown.

Data reduction procedure

A detailed description of the experimental apparatus and the communication procedure for the calculator controlled data acquisition used in testing the compact heat exchanger surface is presented in [1]. The only difference is the software for the data reduction which has been developed to follow the procedure to be explained shortly.

Instead of using strip chart recorder for continuous recording the temperature-time trace, discrete readings of TP0, TP1 and TP2 (refer to Fig. 2 of [1] thermopile temperatures ($Y_{1,n}$, $Y_{2,n}$ and $Y_{\min,n}$ respectively) have been programmed with short time steps between particular readings. At the early stage of the work, the time steps ranging from 0.075 to 0.2 s have been tried and the temperature-time curves have been compared for smoothness with those obtained from the plotter of a continuous recorded that was connected in-parallel to separate channels. The typical discretely recorded temperature histories are presented in Fig. 3. It can be seen that the discrete points determining each curve are sufficiently dense to provide an accurate numerical processing. We are not going to describe the complete story of the corroboration work that would be a chronology of many trial runs leading us to the final decision that the time steps of 0.1 s are sufficiently small for a reliable data reduction procedure. In few words, we arrived at the conclusion that 3×40 temperature readings in the first 12 seconds after the heater has been switched on, as it was in testing the empty test section [1], are quite adequate. The readings of just TP0 and TP2 temperatures $Y_{\min,n}$ and $Y_{2,n}$, respectively, are used for data reduction,

while the temperatures $Y_{1,n}$ of the temperature sensor TP1, located upstream from the matrix, were recorded just for verification that the test section part between the heater and the matrix behaves like an empty test section.

As discussed in [1] , the early stage of transient response was selected for data reduction procedure in order to validate the classical assumptions of heat transfer mechanism and to satisfy the model conditions. Here we have in mind primarily the neglection of the axial conduction effects. It has been shown by Cai *et al.* [4] that the longitudinal conduction effect must be included in the analysis for both $NTU \leq 3$ and $\Lambda NTU \geq 0.06$. Our experimental values of the number of transfer units were in the range $1.48 \leq NTU \leq 3.87$ (the highest value corresponds to the lowest Reynolds number). Longitudinal conduction parameter for our tests has been estimated using the effective thermal conductivity of the cellular sandwich structure of the test core. It has been found that $0.038 \leq \Lambda \leq 0.159$, so that $0.056 \leq \Lambda NTU \leq$ ≤ 0.615 in our experiments. To ensure that these conduction effects can be neglected we have selected just the outlet fluid temperatures being recorded up to the 6th second of the experiment for matching the temperature-time trace according to DFEM. Two dinstinct instants: one corresponding to the 10th and the other to the 20th reading of the TP2 temperatures (see Fig. 3) have been selected for data reduction procedure. Two points in time are needed for the evaluation of two experimental values: NTU and c_S. For that purpose, the Eq. (8) should be collocated at the local time (τ^*_m) values corresponding to the values of the real times τ_{10} and τ_{20} of the 10th and the 20th reading, respectively.

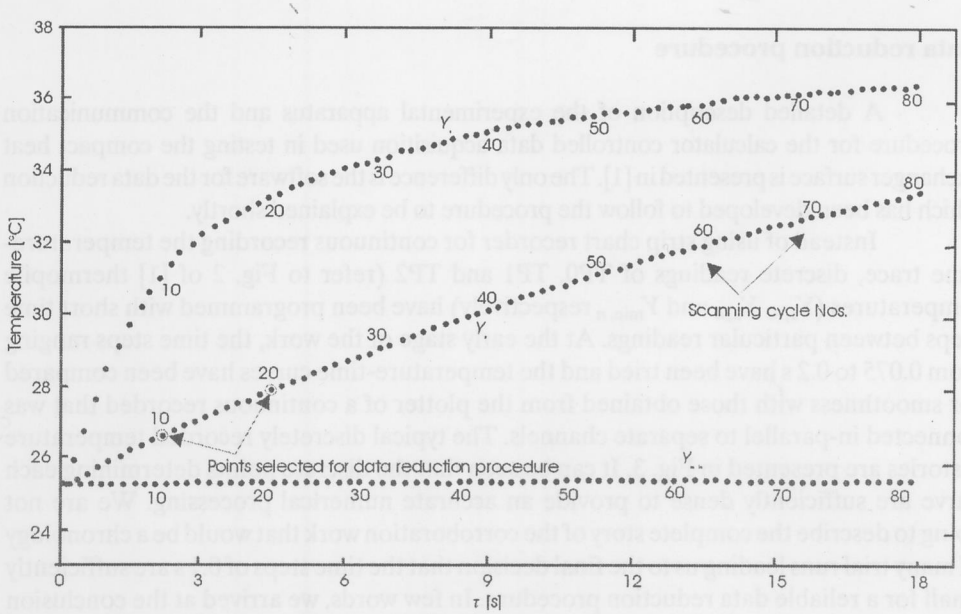

Figure 3. Temperature histories as recorded at 60% of maximal fan speed with time steps $\Delta\tau = 0.075$ s in 80 scanning cycles

To derive the working formula denote the instantaneous fluid outlet temperature $T(L, \tau_m)$ by $T_{out}(\tau)$. Instantaneous fluid temperature rise $T_{out} - T_{\min}$ at the test matrix outlet is not isochronous with its corresponding temperature rise $T_2 - T_{\min}$ at the TP2 location. Since thermopile TP2 is placed $L_0 = L_2 - L_{m2} = 115$ mm apart from the matrix exit, there is a delay equal to the fluid transit time L_0/w. By the time it reaches the TP2 location, temperature rise $T_{ort} - T_{\min}$ is also attenuated by the factor $\exp(-NTU_a L_0 / L_2)$ due to the finite fluid-towall number of transfer units NTU_a. Thus, at any time instant τ the following relation:

$$\left(T_{out} - \overline{T}_{\min}\right)\Big|_{\tau} = e^{\frac{NTU_a L_0}{L_2}} \left(T_2 - \overline{T}_{\min}\right)\Big|_{\tau + L_0/\overline{w}} \tag{10}$$

should be used to predict $T_{out} - T_{\min}$ on the basis of $T_2 - T_{\min}$. In the present experiments this meant that, at the highest Reynolds number. $T_{out} - T_{\min}$ was 2.54% larger than $T_2 - T_{\min}$ after 0.016 s. At the lowest Re_a the corresponding values have been 5.45% and 0.069 s, respectively. However, actual measurements of instantaneous TP2 temperatures Y_2, instead of instantaneous fluid temperatures T_2, as well as the data processing of $Y_2 - T_{\min}$ instead of $T_2 - T_{\min}$, involved further corrections for the temperature sensor time constant τ_{s2} according to the model presented in [1]. Details of this procedure are not given here since our experience proved that a simpleishochronous (at any τ) heat balance equation of the form:

$$\dot{m} c_p \left(T_{out} - Y_2\right) = D_i \pi L_0 \alpha_a \left(\frac{T_{out} + Y_2}{2} - \overline{T}_{\min}\right) \tag{11}$$

can compensate all of the abovementioned effects.

Equation (11) states that the rate of the fluid enthalpy change (corresponding to the cooling from T_{out} to Y_2) is equal to the fluid-to-wall convective heat transfer rate. here, it is assumed that the fluidflowin along the test section part, from the matrix outlet to the TP2 location, is at the mean temperature $(T_{out} + Y_2)/2$, and that the wall is still at the initial temperature $T_{\min}$ as follows from the equation (10) of [1]. By using the definition of the fluid-to-wall number of transfer units, equation (11) can be rewritten in the form:

$$T_{out} - \overline{T}_{\min} = \frac{1+b}{1-b}\left(Y_2 - \overline{T}_{\min}\right) \tag{12}$$

where

$$b = \frac{NTU_a}{2}\frac{L_0}{L_2} \tag{13}$$

This result can be used locally in time for accurate prediction of actual T_{out} values of the basis of Y_2 measurements, $T_{\min}$ as calculated from $Y_{\min,n}$ measurements (see Eq. 23 of [1]), and NTU as calculated from Eq. (40) of the same reference with Re_a corresponding to the flow rate measurement of the particular experimental run.

In accordance with the discussion given above, the data reduction procedure is based on the solution procedure of the following two equations:

$$G_i \equiv \frac{KB(\tau_i)}{c_S} NTU - V_2\left(NTU, \frac{K\tau_i}{c_S} NTU\right) = 0, \quad i = 10{,}20 \tag{14}$$

where

$$K = \frac{\dot{m} c_p}{m_S} \tag{15}$$

and

$$B(\tau_i) = \frac{(1+b)(1-b)}{\Delta T_{\max} \exp(-NTU_a L_{m1} / L_2)} \left[\int_0^{\tau_i} \Delta Y_2(y)dy + \tau_0 \Delta Y_2(\tau_i) \right] \tag{16}$$

with

$$\Delta Y_2 = Y_2 - \overline{T}_{\min} \tag{17}$$

The Newton-Raphson method is used for solving the two equations (14). The iterations are always started with initial guesses $NTU = 2$ and $c_S = 900$ J/kg K), and halted when both $\left|NTU^{new} - NTU^{old}\right| \le 10^{-5}$ and $\left|c_S^{new} - c_S^{old}\right| \le 10^{-2}$. The partial derivatives of the $G_i(NTU, c_S)$ functions, needed for the Newton-Raphson method are:

$$\frac{\partial G_i}{\partial NTU} = \frac{K}{c_S} B(\tau_i) + \left(1 - \frac{K\tau_i}{c_S}\right) V_1\left(NTU, \frac{K\tau_i}{c_S} NTU\right) - V_{1,0}\left(NTU, \frac{K\tau_i}{c_S} NTU\right) \tag{18}$$

and

$$\frac{\partial G_i}{\partial c_S} = \frac{K}{c_S^2} NTU \left[V_1\left(NTU, \frac{K\tau_i}{c_S} NTU\right) - B(\tau_i) \right] \tag{19}$$

Explicit relations for V_1 and $V_{1,0}$ functions appearing in these equations are given in the Appendix.

Appropriate software, being a part of the general communication and computation program for a single run, makes the total duration of the experiment some what longer than it was with the empty apparatus [1]. Typically 3 minutes were needed for the complete run with data reduction procedure and printing the final results: Re_a, $\Delta T_{\max}$, τ_0, NTU_a, Re, Pr, NTU, St, j, f and j/f. The humid air properties are evaluated on-line at $T_{\min} + \Delta T_{\max}/2$ as the reference temperature.

A remark has to be made regarding the determination of the flow friction characteristics. The friction factor f is determined from the fluid static pressure drop across the core *without* correction for entrance/exit and flow acceleration/deceleration losses:

$$f = \frac{D_h}{4L} \frac{2\rho\Delta p}{(\dot{m}/A_0)^2} \tag{20}$$

It is, thus, an apparent friction factor corresponding to the total static pressure drop and incorporating the flow losses at the ends of the test matrix. This is done to simplify the pressure drop prediction for the series of cores that the manufacturer produces with the same core length (L = 93.5 mm) in the air flow direction.

The technique being described is simple and quick to carry out. When all geometrical characteristics and the mass of the test core are known, and the apparatus (including software adaptation) is prepared, some 50 experimental runs with different flow rates can be performed per day. Next section presents the results of one hundred experimental runs with the test core being described above.

Test results

To cover the laminar flow region, one hundred experimental runs have been performed in order to establish the basic flow friction and heat transfer characteristics of the test surface. The test Reynolds numbers are not increased by a constant ratio to obtain equally spaced data points. Instead a random number generator was used to determine fan speed for particular runs. This resulted in the Reynolds number range 385 < Re < 1930 for which the correlations to be presented are valid.

The surface characteristics (the Colbrun j factor and the Fanning friction factor f versus Reynolds number Re) are graphed in Fig. 4. All of the data was fitted by standard

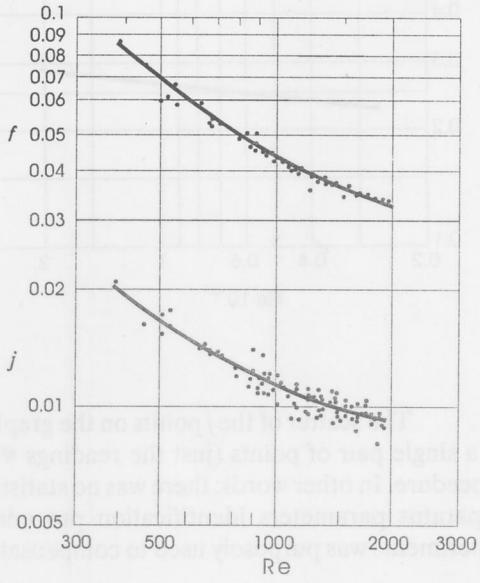

Figure 4. Test core flow friction and heat transfer characteristics

polynomial regression procedure to obtain the best interpretation. Experimental Colburn factor data have been correlated by the following equation:

$$j = 1462\ \mathrm{Re}^{-2.968(1\,-\,0.06179\ \ln \mathrm{Re})} \tag{21}$$

which corresponds to the second order polynomial regression in ln*j* – ln Re coordinates. Experimental apparent Fanning factor data have been correlated by the equation

$$f = 5381\ \mathrm{Re}^{-2.841(1\,-\,0.05833\ \ln \mathrm{Re})} \tag{22}$$

in the region 385 < Re < 1930. Coordinates of the smoothed curves given by Eqs. (21) and (22) are presented in Fig. 4 as well.

Using correlations given by Eqs. (21) and (22) the flow area goodness factor, the *j*/*f* ration, can be established in the form:

$$\frac{j}{f} = 0.2718\ \mathrm{Re}^{-0.1276(1-0.1387\ln \mathrm{Re})} \tag{23}$$

which is a weak function of the Reynolds number as presented in the Fig. 5.

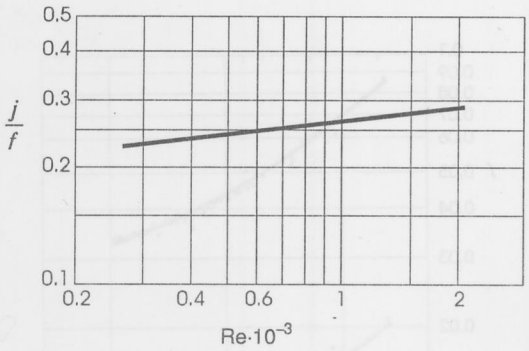

Figure 5. Flow area goodness factor versus Reynolds number

The scatter of the *j* points on the graph in Fig. 4 is a consequence of the selection of a single pair of points (just the readings #10 and #20 of Y_2) for the data reduction procedure. In other words: there was no statistics within a single run as it was in the empty apparatus parameters identification procedure in [1]. However, a large number of experiments was purposely used to compensate this relatively high dispersion in the heat

transfer data. Further refinements of this method, that are presently underway, are tailored to provide much higher determination of the j-Re curve.

The arithmetic mean value of the test core specific heat, based on the complete set of experimental runs, has been found to be c_S = 982.45 J/(kg K) with the standard deviation of ±5.6%. This value is higher than the specific heat of the 99.5% aluminum – the basic material of the heat exchanger core, confirming thus, the effects of the air presence in the cells on the no-flow side of the test core, as well as the brazing composition with different density and specific heat.

The influence of L/D_h on both j-Re and f-Re characteristics is beyond the scope of the present experiments since the test core sample is intended to represent the complete series of the same flow length cores from the manufacturer's production programme.

Acknowledgment

This work was performed as a part of the research supported by the SIZ NR SAP Vojvodine Contract No. 01-804/4 for 1985.

Nomenclature

A [m^2]	– total heat transfer surface area
A_C [m^2]	– matrix cross-sectional area available for heat conduction in flow direction
A_{fr} [m^2]	– frontal area*
A_0 [m^2]	– free flow area*
B (τ_i) [s]	– parameter defined by Eq. (16)
b	– parameter defined by Eq. (13), dimensionles
C_m^*	– fluid to solid matrix thermal capacity ratio, dimensionless*
c_p [J/(kg K)]	– specific heat at constant pressure
c_S [J/(kg K)]	– specific heat of the test core
D_i [m]	– inside diameter of the apparatus tube
D_h [m]	– hydraulic diameter of flow passages*
f	– apparent Fanning friction factor, defined by Eq. (20), dimensionless
G_i	– function of two variables, defined by Eq. (14), dimensionless
I_n	– modified Bessel function of n-th (integer) order
j	– Colburn factor, dimensionless*
K [W/(kg K)]	– relative fluid capacity rate, defined by Eq. (15)
L [m]	– test matrix length in flow direction[m]
L_0 [m]	– test matrix exit to TP2 location distance
L_2 [m]	– apparatus test section length, heater to TP2 distance
L_{m1}[m]	– heater to test matrix inlet location distance
L_{m2} [m]	– heater to test matrix exit location distance

$\dot{m}$ [kg/s] – mass flow rate
m_f [kg] – fluid mass occupying the free flow volume of the test matrix
m_S [kg] – mass of the test core
NTU – number of heat transfer units, dimensionless*
NTU_a – number of fluid-to-wall heat transfer units, dimensionless*
Pr – Prandtl number, dimensionless
Re – Reynolds number based on hydraulic diameter, dimensionless*
Re_a – apparatus Reynolds number, dimensionless*
St – Stanton number, dimensionless
T [°C] – temperature, fluid temperature
T_2 [°C] – fluid temperature at TP2 location
$\overline{T}_{min}$ [°C] – statistical mean minimum temperature in the system
T_S [°C] – solid matrix temperature
T_{out} [°C] – fluid temperature at the matrix outlet*
TP0, TP1, TP2 – designate thermopiles upstream of the heater, upstream of the matrix and downstream of the matrix, respectively
V_1, V_2, $V_{1,0}$ – special functions of two variables, defined in the Appendix
$\overline{w}$ [m/s] – mean fluid velocity through the apparatus tube
x – coordinate along the flow direction measured from the matrix inlet, m also, the first argument of the V functions in the Appendix, dimensionless
Y_1 [°C] – temperature of TP1 sensor
Y_2 [°C] – temperature of TP2 sensor
Y_{min} [°C] – temperature of TP0 sensor
$Y_{1,n}$ [°C] – discrete value of TP1 temperature
$Y_{2,n}$ [°C] – discrete value of TP2 temperature
$Y_{min,n}$ [°C] – discrete value of TP0 temperature
y [s] – dummy variable of the integration with respect to time, also, the second argument in the V functions in the Appendix, dimensionless
α [W/(m^2 K)] – fluid-to-test surface heat transfer coefficient
α_a [W/(m^2 K)] – fluid-to-wall heat transfer coefficient
Δ_p [Pa] – fluid static pressure drop across the test core
ΔT_{max} [°C] – maximum fluid temperature rise
ΔT^* [°C] – maximum fluid temperature rise at the matrix inlet, defined by Eq. (9)
ΔY_2 [°C] – TP2 thermopile temperature rise, defined by Eq. (17)
$\Delta\tau$ [s] – time step between successive temperature readings
θ – dimensionless fluid temperature*
θ_S – dimensionless solid matrix temperature*
Λ – longitudinal conduction parameter, dimensionless*
λ [W/(m K)] – thermal conductivity of the fluid
$\overline{\lambda}$ [W/(m K)] – effective thermal conductivity of the test matrix
μ [Pa s] – viscosity
$\xi = x/L$ – dimensionless coordinate
η – dimensionless local time variable*
η_0 – dimensionless time constant of the exponential inlet fluid temperature signal*
η^* – any particular value of the dimensionless time variable
ρ [kg/m^3] – fluid density

σ – ratio of the free flow area to frontal area, dimensionless
τ [s] – time variable
τ_i [s] – particular value of the time variable
τ_m [s] – matrix local time variable
τ^*_m [s] – any particular value of the matrix local time variable
τ_{S2} [s] – time constant of the TP2 thermopile
τ_0 [s] – time constant of the exponential inlet fluid temperature signal
τ_{10} [s] – value of the time variable at the 10th reading of TP2 temperature
τ_{20} [s] – value of the time variable at the 20th reading of TP temperature

*

$A_{fr} = D_i^2 \pi / 4$
$A_0 = \rho A_{fr}$
$C_m^* = m_f c_p / (m_s c_s)$
$D_h = 4A_0 L/A$
$j = \mathrm{St}\mathrm{Pr}^{2/3}$
$m_f = \rho A_0 L$
$NTU = \alpha A / (\dot{m} c_p)$
$NTU_a = \alpha_a D_i \pi L_2 / (\dot{m} c_p)$
$\mathrm{Pr} = \mu c_p / \lambda$
$\mathrm{Re} = D_h \dot{m} / A_0 \mu$
$\mathrm{Re}_a = \rho \bar{w} D_i / \mu$
$\mathrm{St} = \alpha A_0 / (\dot{m} c_p)$
$T_{out} = T(L, \tau_m)$
$\theta = (T - \bar{T}_{\min}) / \Delta T^*$
$\theta_S = (T_S - \bar{T}_{\min}) / \Delta T^*$
$\Lambda = \lambda A_C / (\dot{m} c_p L)$
$\eta = \dot{m} c_p \tau_0 / (m_s c_s)$
$\eta_0 = \dot{m} c_p \tau_0 / (m_s c_s)$

Appendix

Special functions of two variables x and y (both non-negative), appearing in this paper are:

$$V_{1,0}(x,y) = \mathrm{e}^{-x-y} I_0\left(2\sqrt{xy}\right)$$

$$V_1(x,y) = \mathrm{e}^{-x-y} \sum_{n=0}^{\infty} \left(\frac{y}{x}\right)^{\frac{n}{2}} I_n\left(2\sqrt{xy}\right)$$

$$V_2(x,y) = \mathrm{e}^{-x-y} \sum_{n=1}^{\infty} n \left(\frac{y}{x}\right)^{\frac{n}{2}} I_n\left(2\sqrt{xy}\right)$$

References

[1] Bačlić, B. S., Gvozdenac, D. D., Vadlja, Dj., Performance Identification of the Apparatus for Testing Compact Heat Exchanger Surfaces, *Symposium on Advances in Heat Exchangers at 1986 ASME WAM*, (Eds., R.K. Shah, J.T. Pearson), Anaheim, CA, December 7–12, 1986

[2] Bačlić, B. S., Heggs P. J., Abou Ziyan, H. Z. Z., Differential Fluid Enthalpy Method for Predicting Heat Transfer Coefficients in Packed Beds, *8th International Heat Transfer Conference*, San Francisco, August 17–22, 1986, pp.12

[3] Bačlić, B. S., Heggs, P. J., On the Search for New Solutions of the Single-Pass Crossflow Heat Exchanger Problem, *Int. J. Heat Mass Transfer, 28* (1985), pp. 1965–1976
[4] Cai, Z. H., Li, M. L., Wu, Y. W., Ren, H. S., A Modified Selected Point Matching Technique for Testing Compact Heat Exchanger Surfaces, *Int. J. Heat Mass Transfer, 27* (1984), pp. 971–978

Authors addreess:

Prof. Dr. B. Bačlić, Prof. Dr. D. Gvozdenac, Prof. Dr. D. Sekulić
Institute of Fluid, Thermal and Chemical Engineering
Mechanical Engineering Department, Faculty of Technical Sciences
University of Novi Sad
6, Trg Dositeja Obradovića
21121 Novi Sad, Yugoslavia